Junction and drop-shaft boundary conditions for modeling free-surface, pressurized, and mixed free-surface pressurized transient flows

Arturo S. León [1], Xiaofeng Liu [2], Mohamed S. Ghidaoui [3],
Arthur R. Schmidt [4], Marcelo H. García [5]

Abstract

A junction and drop-shaft boundary conditions (BCs) for one-dimensional modeling of transient flows in single-phase conditions (pure liquid) are formulated, implemented and their accuracy are evaluated using two Computational Fluid Dynamics (CFD) models. The BCs are formulated for the case when mixed flows are simulated using two sets of governing equations, the Saint Venant equations for the free surface regions and the compressible water hammer equations for the pressurized regions. The proposed BCs handle all possible flow regimes and their combinations. The flow in each pipe can range from free surface to pressurized flow and the water depth at the junction or drop-shaft can take on all possible levels. The BCs are applied to the following three cases: a three-way merging flow, a three-way dividing flow and a drop-shaft connected to a single-horizontal pipe subjected to a rapid variation of the water surface level in the drop-shaft. The flow regime for the first two cases range from free surface to pressurized flows, while for the third case, the flow regime is pure pressurized flow. For the third case, laboratory results as well as CFD results were used for evaluating its accuracy. The results suggest that the junction and drop-shaft boundary conditions can be used for modeling transient free surface, pressurized, and mixed flow conditions with good accuracy.

Subject headings: Boundary conditions; Combined sewers; Computational Fluid Dynamics; Mixed flow; Open channel flow; Pressurized flow; Sewer; Transient flow; Unsteady flow; Water hammer flow

Introduction

Boundary Conditions (BCs) in most storm-sewer systems are complicated by the presence of different flow regimes; pure free surface flows (also called open-channel flows), pure pressurized flows, and the simultaneous occurrence of free surface and pressurized flows (mixed flows) [(1), (3) and (2) in Fig. 1, respectively]. When simulating mixed flows, one or two sets of governing equations are used. When using a single set of equations (Saint-Venant equations), an approximation for simulating pressurized flows is needed. The most common approximation for simulating pressurized flows is to use the well-known Preissmann slot, which consists of a hypothetical narrow open-slot on top of the conduit (e.g., Garcia-Navarro et al. (1994), Capart et al. (1997), León et al. (2009a)).

The boundary conditions in mixed flow conditions when using the Preissmann slot approach are the same as those of free surface flows. The main limitation of the Preissmann approach is its inability to simulate sub-atmospheric pressures in pressurized flow conditions. To overcome this limitation, Vasconcelos et al. (2006)

[1] Assistant Professor, Civil Engineering, Boise State University, 1910 University Drive, Boise, ID 83725-2075, USA. E-mail: arturoleon@boisestate.edu (Corresponding author)
[2] Post-doctoral Research Associate, Civil and Environmental Engineering, University of Illinois, 205 N. Mathews Ave., Urbana, IL 61801, USA. E-mail: liu19@illinois.edu
[3] Professor, Civil Engineering, The Hong Kong University of Science and Technology, Room 3569, Clear Water Bay, Kowloon, Hong Kong. E-mail: ghidaoui@ust.hk
[4] Research Assistant Professor, Civil and Environmental Engineering, University of Illinois, 205 N. Mathews Ave., Urbana, IL 61801, USA. E-mail: aschmidt@illinois.edu
[5] Professor, Civil and Environmental Engineering, University of Illinois, 205 N. Mathews Ave., Urbana, IL 61801, USA. E-mail: mhgarcia@illinois.edu

modified the Saint-Venant equations to allow for over-pressurization. The main limitation of this approach is the presence of what these authors call “post shock oscillations”. To keep these oscillations small, lower values for the pressure wave celerity may be used, however this may compromise the accuracy of the simulation if pressurized transients are simulated.

Although the mathematical and numerical formulation of mixed flows using one single set of equations are much simpler than those using two sets of equations, it appears that the latter produce less numerical problems, especially when large pressure wave celerities are used (León and Ghidaoui (2010)). Regardless of the method used, the correct pressure wave celerity must be used when transient flows are of interest (León and Ghidaoui (2010)).

Unlike for pure free surface flows (or mixed flows using the Preissmann slot approach) and pure pressurized flows, for which vast literature on boundary conditions exists (e.g., Sjöberg (1976), Yen (1986), McInnis (1992), Garcia-Navarro et al. (1994), Capart et al. (1999), León et al. (2006), Ridgway and Kumpula (2006), León et al. (2008)), the mixed-flow literature when using two sets of governing equations has focused on internal solutions, such as the Method of Characteristics or Finite Volume method (e.g., Song et al. (1983), Cardle (1984), León (2006), Bourdarias and Gerbi (2007), Politano et al. (2007), León et al. (2010)) but there is little work devoted to BCs. The current formulations for mixed flows at boundaries when using two sets of governing equations (e.g., Song et al. (1983), Politano et al. (2007)) are not general, and can not handle positive and negative mixed flow interfaces for all flow conditions (e.g., a negative mixed flow interface with supercritical flow in the free surface region). Song et al. (1983) defined a mixed flow interface as positive if it is moving towards the open-channel flow, and negative or retreating if it is moving towards the region of pressurized flow. The change in direction of the

interface from positive to negative is called interface reversal.

Perhaps the most common boundary in storm-sewer systems is a junction connected to an arbitrary number of pipes. A junction boundary may be connected to several pipes and the flow at the boundary may be multi regime, which means that the flow between the junction pond and each of the connecting pipes may be in free surface, pressurized or mixed flow regime. The fact that a junction boundary may be multi regime and may be connected to multiple pipes makes the treatment of this boundary condition much more difficult than a single pipe that has a mixed flow interface inside the pipe. Because a junction boundary is very common in storm-sewer systems, a robust and accurate approach for the treatment of this type of boundary is necessary.

A drop-shaft is another common boundary in storm-sewer systems. Guo and Song (1991) simulated pure pressurized flows in a drop-shaft connected to a single-horizontal pipe and subjected to a rapid variation of water surface level in the drop-shaft, using three equations for solving the flow variables at the drop-shaft boundary. These were the steady energy equation, a combined mass and y-momentum equation, and an equation based on the Method of Characteristics (MOC). These equations were used by the authors of the present paper for test case 3 (oscillation tube), but were found to result in numerical instabilities that grew rapidly and caused the abortion of the program. Because a drop-shaft boundary is very common in storm-sewer systems, a robust and accurate approach for the treatment of this type of boundary is necessary.

This work is motivated by the fact that BCs are important but analysis is lacking for mixed transient flows when using two sets of governing equations. As mentioned earlier, a junction connected to an arbitrary number of pipes and a drop-shaft are perhaps the most common boundaries in storm-sewer systems. Hence, the present

work focus on formulations for the treatment of these boundaries. For consistency and for completeness, boundary conditions for all flow regimes (free surface, pressurized and mixed flows) are presented herein. Most of the equations presented in this paper were reproduced, adapted or reformulated from the literature with the aim of simulating all possible flow regimes. For mixed flow conditions, no approach similar to that presented in this paper was used before at boundaries. As mentioned earlier, several authors (e.g., Song et al. (1983), Cardle (1984), Bourdarias and Gerbi (2007) and León et al. (2010)) presented solutions for mixed flow interfaces at internal cells (inside of a pipe), however this approach was not used at boundaries before. When a pipe is subjected to mixed flow conditions at its boundary, the approach used herein is similar to that used for mixed flow interfaces at internal cells (e.g., Song et al. (1983), Cardle (1984), Bourdarias and Gerbi (2007) and León et al. (2010)).

The proposed boundary conditions have been implemented in the Illinois Transient Model (ITM) [León et al. (2009b)], which was used for the computations of the present study. The ITM model is an open source code Finite Volume (FV) model intended for analyzing transient and non-transient flows in closed-conduit systems ranging from dry-bed flows, to gravity flows, to partly gravity-partly surcharged flows to fully pressurized flows (waterhammer flows).

This paper is organized as follows: (1) a BC formulation for a N-way junction (N pipes) is presented; (2) a BC formulation for pure pressurized flows in a drop-shaft connected to a single-horizontal pipe that is subjected to a rapid variation of the water surface level in the drop-shaft is presented; (3) a brief overview of two state-of-the-art three-dimensional Computational Fluid Dynamics (CFD) models is presented; (4) the accuracy of the junction and drop-shaft boundary conditions are evaluated by comparison to CFD modeling experimental results; and (5) the results

are summarized in the conclusion.

Formulation of Boundary Conditions

In a typical storm-sewer system, various types of boundaries are present. These may include drop-shafts, reservoirs, junctions, dead ends, control gates, etc. As mentioned earlier, a junction connected to an arbitrary number of pipes and a drop-shaft are perhaps the most common boundaries in storm-sewer systems. Hence, the present work focus on formulations for the treatment of these boundaries. These formulations are described below. The proposed approach for boundary conditions has the limitations of all one-dimensional models. For instance, at junctions, the energy losses are simply simulated using empirical head losses between the junction pond and each connecting pipe.

N-way junction boundary

A N-way junction boundary (N pipes) is depicted schematically in Fig. 2 and consists of "p" inflowing pipes and "q" outflowing pipes, with $N = p + q$. A pipe is denoted as inflowing (or outflowing) when it conveys flow to (or from) the boundary under normal-flow conditions (e.g., uniform flow). If a pipe has zero longitudinal slope, the pipe can be treated as either inflowing or outflowing. In a N-way junction boundary, $2N + 1$ variables are unknown, namely, the piezometric depth (y_b) and the flow discharge (Q_b) at each pipe boundary, and the water depth at the junction pond (y_d). Rigorously, not always two variables at each pipe boundary would be required. For instance for an inflowing pipe in supercritical flow conditions (e.g., downstream boundary), y_b and Q_b are not needed. However, the proposed formu-

lation is intended to be general and in all cases $2N + 1$ equations will be solved. This is not a problem for an inflowing pipe in supercritical flow conditions because in this case the solution of the proposed equations will give that the flow conditions at the boundary (new time step) are the same as those of the cell located right upstream of the boundary at the previous time step, and therefore will not affect the supercritical flow upstream of the boundary as expected. It is acknowledged that all flow variables that are not constant (e.g., gravity wave celerity) can be expressed as a function of either y, Q or both. Thus, $2N + 1$ equations are needed in order to determine the unknown variables. To obtain $2N + 1$ equations, two equations are required for each pipe ($2N$) and an additional equation is needed at the junction pond (1). The two equations suggested at each pipe boundary for each type of flow are presented next.

Free surface flow: For a pure free surface flow, the first equation is obtained by using the Riemann invariants between the pipe boundary and the first cell of the corresponding pipe adjacent to the junction pond. The differential relationships of the generalized Riemann invariants for free surface and pressurized flows can be written as d$u\pm$ (c/A)dA = 0 and d$u\pm$ a d($\rho_f A_f$)/($\rho_f A_f$) = 0, respectively (e.g., León et al. (2008), León et al. (2009a)). In the latter relations, u is the flow velocity, c is the gravity wave celerity, A is the cross-sectional area of flow (free surface flow), a is the pressure wave celerity, ρ_f is the fluid density in pressurized flow conditions (variable) and A_f is the full cross-sectional area of the conduit. The Riemann invariants for free surface flows are approximated by integrating the differential relationships provided by the generalized Riemann invariants using the trapezoidal rule (León et al. (2009a)). This relationship is given by [León et al. (2009a)]

$$u_{b_j}^{n+1} - u_j^n \pm (c_{b_j}^{n+1} + c_j^n) \frac{A_{b_j}^{n+1} - A_j^n}{A_{b_j}^{n+1} + A_j^n} = 0 \tag{1}$$

where the positive sign (+) in Eq. (1) is used for inflowing pipes (e.g., pipes 1 and 2 in Fig. 2) and the negative sign (-) for outflowing pipes (e.g., pipes 4 and 5 in Fig. 2). In Eq. (1), the subscript b refers to boundary and j (j = 1, 2, ...) identifies the pipe. Note in Eq. (1) that c and A are a function of only y, and u is a function of Q and y. As mentioned earlier, all flow variables that are not constant can be expressed as a function of either y, Q or both.

The concept of Riemann invariants is similar to the Method of Characteristics. The reader is referred to Toro (2001) for a detailed description of the concept of Riemann invariants. The reader may question the validity of Eq. (1) given that Riemann invariants are truly constant along characteristic curves only for a frictionless system, however this approximation is used only at the boundaries in the ITM model (used for the preparation of the paper). In the ITM model, the friction at internal cells is taken into account through time splitting (see León et al. (2010)). Thus, the frictionless assumption at the boundaries may not affect significantly the accuracy of the solution. Eq. (1) can be used for all free surface flow conditions, except for the case of an outflowing pipe that has supercritical flow moving downstream (case (3) in Fig. 3(b)). In this case the characteristic "$u - c$" does not cross the boundary and therefore the Riemann invariants can not be used, so Eq. (1) is replaced by a critical flow depth condition at the outflowing pipe boundary. For case (1) in Fig. 3(a) [inflowing pipe], the characteristic "$u + c$" does not cross the boundary, and therefore the concept of Riemann invariants can not be used across this characteristic. However, a supercritical flow moving upstream is not possible for an inflowing pipe. Thus for an inflowing pipe, the concept of Riemann invariants can be used for all flow conditions.

For a pure free surface flow, an inflowing pipe may be coupled or decoupled from the junction boundary. It is denoted coupled if the flow at the pipe boundary is influenced by flow conditions at the junction pond, and decoupled otherwise. For instance if there is a drop at the junction (junction pond invert is lower than inflowing pipe invert) and the water elevation in the junction pond is low compared to the water elevation in the inflowing pipe, there is free surface flow discontinuity between the junction pond and the inflowing pipe (e.g., Yen (1986)). In the decoupled case, the concept of Riemann invariants still can be used because the Riemann invariants connect the flow variables at the boundary of a given pipe with an internal cell adjacent to the same pipe. The application of Riemann invariants is independent from the water depth in the junction pond.

The second equation for pure free surface flows is presented for inflowing and outflowing pipes separately. For an inflowing pipe, the second equation is given by [e.g., Yen (1986), Yen (2001)]

- When the inflowing pipe is decoupled from junction boundary (j = 1, p)
  - For subcritical flow (decoupled when $dr_j + y_{c_j} > y_d$, otherwise is coupled)

$$y_{b_j} = y_{c_j} \tag{2}$$

  - For supercritical flow (decoupled when $dr_j + y_{\text{conj}_j} > y_d$, otherwise is coupled)

$$y_{b_j} = y_{u_j} \tag{3}$$

- When inflowing pipe is coupled with junction boundary (j = 1, p)

$$dr_j + y_{b_j} + \frac{u_{b_j}^2}{2g} - k_j \frac{u_{b_j}|u_{b_j}|}{2g} = y_d \tag{4}$$

where y_c is the critical depth, y_{u_j} is the flow depth in pipe j right upstream the junction boundary (i.e., flow depth in cell adjacent to the boundary), y_{conj} is the conjugate depth associated with y_u, k is the local head loss coefficient and dr is the drop height between a pipe invert and junction pond bottom. It is pointed out that unless k is specified as 1, there will be some conditions for which there is no solution to Eq. (4). These conditions may occur when the flow at a boundary is near to critical flow conditions. However, this is not of practical importance because if it happens (e.g., boundary pressurization from downstream when the flow upstream of the boundary is near critical conditions), it occurs only for few time steps (few seconds). The no convergence is not of concern for the ITM model (Finite Volume model) because whenever there is no convergence at the boundary the old time flux is used at this location.

For an outflowing pipe, the second equation is the same as Eq. (4) [energy equation], except for the sign of the term $k_j \frac{u_{b_j}|u_{b_j}|}{2g}$. In general the energy equation can be written as

$$dr_j + y_{b_j} + \frac{u_{b_j}^2}{2g} \mp k_j \frac{u_{b_j}|u_{b_j}|}{2g} = y_d \tag{5}$$

where the negative sign (-) in Eq. (5) is used for inflowing pipes and the positive sign (+) for outflowing pipes.

Pressurized flow: As for the case of a pure free surface flow, in a pure pressurized flow, the first equation is obtained by using the Riemann invariants between the pipe boundary and the first cell of the corresponding pipe adjacent to the junction pond. This equation is given by [León et al. (2010)]

$$u_{b_j}^{n+1} \pm a \ln(\rho_f A_f)_{b_j}^{n+1} - (u_j^n \pm a \ln(\rho_f A_f)_j^n) = 0 \tag{6}$$

where the positive sign (+) in Eq. (6) is chosen for inflowing pipes and the negative sign (-) for outflowing pipes.

The second equation in pure pressurized flow conditions is the same as Eq. (5).

Mixed flow: As mentioned earlier, when a connecting pipe is subjected to mixed flow conditions at its boundary, the approach used herein is similar to that used for mixed flow interfaces at internal cells (e.g., Song et al. (1983), Cardle (1984), Bourdarias and Gerbi (2007) and León et al. (2010)). In this paper, the equations in León et al. (2010) for mixed flow interfaces at internal cells are used for a connecting pipe that is subjected to mixed flow conditions at its boundary. These equations are obtained by enforcing mass, momentum and energy relations across the mixed flow interfaces and Riemann solvers at the sides of the interfaces. As is shown in León et al. (2010), this approach can handle all possible mixed flow conditions (e.g., a positive mixed flow interface approaching a non-surcharged junction, depressurization of the junction [negative interface propagating into a pipe]) and has the ability of simulating mixed flows when using realistic pressure wave celerities ($a\sim$ 1000 m/s). As defined earlier, a mixed flow interface is positive if it is moving towards the open-channel flow, and negative or retreating if it is moving towards the region of pressurized flow.

To avoid redundancy and due to space limitations the equations presented in León et al. (2010) are not repeated herein. However, it should be straight forward to identify in León et al. (2010) the equations that need to be used for each condition. For instance for a positive mixed flow interface (shock) at a pipe boundary propagating inside the pipe (called positive interface propagating upstream in León

et al. (2010)), Eqs. (12), (13) and (18) in León et al. (2010) are solved to obtain the flow variables (or fluxes) at the mixed flow boundary. Eqs. (12), (13) and (18) are equations of conservation of mass across the interface, conservation of momentum across the interface and Riemann invariants in the pressurized flow region, respectively.

For a negative mixed flow interface at a pipe boundary propagating inside the pipe (called negative interface propagating upstream in León et al. (2010)), the flow variables at the boundary are determined in two steps. In the first step, Eqs. (12), (13), (19), and (20) in León et al. (2010), which conserve mass, momentum and energy across the interface and use the concept of Riemann invariants in the pressurized flow region, are solved to obtain the flow variables at the left of the boundary ($\mathbf{U}_+$ in León et al. (2010). In the second step, an open channel flow Riemann problem is solved using the HLL (Harten, Lax and Van Leer) solver (see León et al. (2010)), which handles subcritical and supercritical flows automatically (Toro (2001)).

The approach described above provides two flow variables at the boundary for each pipe (A_{b_j} and Q_{b_j} for j = 1, 2, ... N). Because the computation of these variables in mixed flow conditions is time consuming, these variables (A_{b_j} and Q_{b_j}) are determined at the old time step ($t = n$) and they are assumed to hold at the new time step ($t = n + 1$). Hence, if "r" pipes have mixed flow interfaces at a junction boundary, only $2(N - r) + 1$ equations need to be solved by iteration.

Until now we have two equations for each pipe (inflowing or outflowing) having a total of $2N$ equations. The last equation ($2N + 1$) is obtained from mass balance at the junction pond, which can be written as

$$\frac{(Q_d^{n+1} + Q_d^n)}{2} - \frac{(Q_o^{n+1} + Q_o^n)}{2} + \sum_{j=1,N} \frac{(Q_{b_j}^{n+1} + Q_{b_j}^n)}{2} = A_d \frac{dy_d}{dt} \tag{7}$$

where Q_d is an inflow discharge that enters the junction pond at its top (Fig. 2), Q_o is the overflow discharge. The overflow discharge when the inertia of the backflow in the junction pond is negligible can be estimated using the weir equation as follows: Q_o = 0, if $y_d \leq y_o$, and $Q_o = CB(y_d - y_o)^{3/2}$, if $y_d > y_o$, in which y_d = water depth above drop-shaft bottom, C = weir discharge coefficient, and B = weir length.

The boundary condition presented in this section can be used for a junction connected to any number of inflowing or outflowing pipes and any vertical alignment. As an example of using this boundary, consider a three-way merging flow boundary, which consists of two inflowing pipes (e.g., pipes 1 and 2) and one outflowing pipe (pipe 3). Furthermore, assuming that the flow type (between the junction pond and the first cell in the pipe adjacent to the junction pond) is free surface for pipe 1, mixed for pipe 2, and pressurized for pipe 3. In this case, Eqs. (1) and (2) [or (3), or (4)] are used for pipe 1, the equations presented in León et al. (2010) are used for pipe 2, and Eqs. (5) and (6) are used for pipe 3. The last equation used is Eq. (7). It is repeated that in mixed flow conditions, the computation of the boundary flow variables is time consuming, and thus, the flow variables in mixed flow conditions are determined at the old time step ($t = n$) and they are assumed to hold at the new time step ($t = n + 1$). Hence, if "r" pipes have mixed flow interfaces at a junction boundary, only $2(N - r) + 1$ equations need to be solved by iteration. The resulting system of equations can be solved using the Newton-Raphson method. Typically between three to five iterations are needed for achieving convergence.

Drop-shaft boundary subjected to a rapid variation of its water surface level

In the previous section we presented a BC formulation for a junction connected to any number of inflowing or outflowing pipes and any vertical alignment. In this

section we present a methodology for simulating pressurized flows in a drop-shaft subjected to a rapid variation of its water surface level. For simulating free surface and mixed flow conditions in drop-shafts, the same approach presented in the previous section can be used.

As depicted in Fig. 4, a drop-shaft consists of a vertical shaft connected to a near-horizontal tunnel. For a drop-shaft boundary connected to a single tunnel, three variables are unknown, namely, the water depth at the drop-shaft (y_d), and the piezometric depth (y_b) and flow discharge (Q_b) at the outlet pipe boundary. Thus, three equations are needed in order to determine the unknown variables.

As mentioned in the introduction, the approach of Guo and Song (1991) was applied for test case 3 (oscillation tube subjected to rapid variation of their water surface levels), but was found to result in numerical instabilities that grew rapidly and caused the abortion of the program. For determining the three above mentioned flow variables, Guo and Song (1991) used the steady energy equation, a combined mass - y-momentum equation, and an equation based on the Method of Characteristics (MOC). In order to overcome the numerical instabilities produced when using these equations, the equations used by Guo and Song (1991) were reformulated. The new set of equations, which were found to be robust and to provide accurate results, are presented next.

In a similar way to the N-way junction boundary for the pressurized flow case, the first equation is obtained by using the Riemann invariants between the pipe boundary and the first cell of the pipe adjacent to the drop-shaft. This equation is given by [León et al. (2010)]

$$u_b^{n+1} - a\ln(\rho_f A_f)_b^{n+1} - (u^n - a\ln(\rho_f A_f)^n) = 0 \tag{8}$$

Eq. (8) is based on the concept of Riemann invariants and is used for consistency with the N-way junction boundary condition. When using the equation based on the MOC approach instead of Eq. (8), identical results are obtained, so that neither the MOC nor the Riemann invariants are the source of the aforementioned instability problems mentioned above.

The second equation used is the conservation of mass in the drop-shaft, which can be written as

$$Q_d - Q_b = A_d \frac{dy_d}{dt} \tag{9}$$

which is discretized as

$$\frac{(Q_d^{n+1} + Q_d^n)}{2} - \frac{(Q_b^{n+1} + Q_b^n)}{2} = A_d \frac{{y_d}^{n+1} - {y_d}^n}{\Delta t} \tag{10}$$

The third equation used is the y-momentum equation which can be written as

$$-\frac{d}{dt}(Q_b y_d) + \frac{Q_d^2}{A_d} = -gA_d y_d + gA_d y_b + g\pi \sqrt[3]{4} n_m^2 D^{2/3} y_d \frac{Q_b|Q_b|}{A_d^2} \tag{11}$$

where n_m is the Manning's roughness coefficient, the terms $gA_d y_d$ and $gA_d y_b$ are $1/\rho$ times the weight of the water in the drop-shaft and the pressure force at the bottom of the drop-shaft (see Fig. 4), respectively. Eq. (11), which was derived by making the hydrostatic pressure assumption, is discretized as

$$-\left(\frac{Q_b^{n+1}{y_d}^{n+1} - Q_b^n {y_d}^n}{\Delta t}\right) + \frac{(\frac{Q_d^{n+1}+Q_d^n}{2})^2}{A_d} = -gA_d \frac{{y_d}^{n+1} + {y_d}^n}{2} + gA_d \frac{y_b^{n+1} + y_b^n}{2} + g\pi \sqrt[3]{4} n^2 D^{2/3} \Big(\frac{{y_d}^{n+1} + {y_d}^n}{2}\Big) \frac{\Big(\frac{Q_b^{n+1}+Q_b^n}{2}\Big)\Big|\frac{Q_b^{n+1}+Q_b^n}{2}\Big|}{A_d^2} \tag{12}$$

Unlike the approach of Guo and Song (1991), the steady energy equation is not used and the mass and y-momentum equations are not combined into one equation but rather used independently. While boundary conditions for drop-shafts could be developed using the mass, steady energy equation and Riemann invariant (or MOC-based) equations, it will be shown later (test case 3) that when a drop-shaft is subjected to a rapid variation of its water surface level, the flow inertia in the drop-shaft may need to be taken into account for an accurate prediction of the frequency of the water surface level oscillations. The flow inertia can be taken into account using the y-momentum equation or the unsteady form of the energy equation but not using the steady energy equation. In the proposed formulation for drop-shafts, the losses are assumed to be due entirely to wall friction.

Computational Fluid Dynamics (CFD) Modeling

With the aim of evaluating the junction and drop-shaft boundary conditions, CFD modeling results were used as a basis of comparison. Two CFD codes were used in this paper, namely FLOW-3D (Flow Science (2005)) and OpenFOAM (OpenCFD (2007)). FLOW-3D is a commercial CFD package that uses the finite volume (FV) method to solve the Reynolds-Averaged Navier-Stokes (RANS) equations. In this code, the computational domain is subdivided using Cartesian coordinates into a grid of variable-sized hexahedral cells. To represent obstacles FLOW-3D uses the Fractional Area/Volume Obstacle Representation (FAVOR) method, which is outlined by Hirt and Sicilian (1985) and Hirt (1985). The k-ϵ model, as outlined by Rodi (1980), was used for turbulence closure. OpenFOAM is an open source CFD code that provides a library of solvers (for incompressible and compressible flows, multiphase flows, etc.) and a platform to implement new solvers for the solution of a wide array of problems. When using the OpenFOAM framework, the governing

equations for a given problem are discretized using a FV method and they need to be specified in a tensorial partial differential equation form. The implementation details of the code can be found in Jasak (1996). OpenFOAM uses an unstructured mesh. Therefore it is easy to model complex domains and there is no need to use fractional area/volume to represent obstacles as in Flow-3D. For consistency with the package FLOW-3D, a k-ϵ model was also used for turbulence closure when using OpenFOAM.

Evaluation of the model

Because of the lack of experimental data for the flows of interest in complex boundaries (e.g., junction), the first two test cases presented herein consider hypothetical tests, namely a three-way merging flow system and a three-way dividing flow system. A three-way merging flow consists of two inflowing pipes and one outflowing pipe and a three-way dividing flow boundary consists of one inflowing pipe and two outflowing pipes. The third test case involves flow in an oscillation tube for which experiments were performed by the authors. In the first two test cases, the lengths of the pipes are intentionally chosen to be short so that the boundaries have a clear effect on the results. The FLOW-3D results were used as benchmark for the first two test cases and both OpenFOAM and experimental results were used for the third test case. Unlike OpenFOAM, FLOW-3D allows modeling of acoustic waves in pressurized flow conditions. The propagation of acoustic waves is associated with the compressibility of the flow; however not all CFD compressible models can simulate acoustic waves. In the first two test cases, piezometric depths inside horizontal pipes are of interest, for which modeling of acoustic waves is important if pressurized flows are present. In the third test case, even when fully pressurized flows are simulated, modeling of acoustic waves is not important because in this test

the interest is water level oscillations at drop-shafts (vertical pipes) and not piezometric depths inside the horizontal pipe. The main reason for using OpenFOAM in the third test case is that the unstructured mesh used by OpenFOAM allows a better representation of the pipe geometry (e.g., cross-sectional area) than the Cartesian mesh used by FLOW-3D.

Three-way merging flow

The hypothetical test presented in this section considers a three-way merging flow system that is depicted in Fig. 5(a). As shown in Fig. 5(a), all pipes have a length of 5 m, the junction pond has a diameter of 1 m, the inflowing pipes (pipes 1 and 2) have both a diameter of 0.5 m and the outflowing pipe (pipe 3) has a diameter of 0.8 m. The Manning's roughness coefficient used in the 1D simulation is n_m = 0.015 $m^{1/6}$ (for an explanation of why the units of n_m is $m^{1/6}$ see Yen (1991)), the head loss coefficient (k) assumed at the inlet and outlet of the pond is 0.5, the waterhammer wave speed considered is 100 m/s and the initial flow velocity in all pipes is 0 m/s. A waterhammer wave speed of 100 m/s was used because of PC hard disk storage limitations (200 GB) when running FLOW-3D. For instance when using a mesh of 6,000,000 cells, a pressure wave celerity of 100 m/s, an output time of 0.001 s (to be able to capture the piezometric depth traces associated with a pressure wave celerity of 100 m/s) and a total simulation time of 0.2 seconds, the storage required in the PC was about 150 GB. Given the PC hard disk storage limitations, it was decided to use a maximum pressure wave celerity of 100 m/s in this and the next test case.

It is emphasized that the pressure wave celerity is not a limitation of the ITM model. In fact this model was used for simulating the test case under consideration for pres-

sure wave celerities of 500 and 1000 m/s (results not shown). When using the ITM model, the solutions for free surface flows were identical to those obtained using a celerity of 100 m/s, where as for pressurized flows, as expected, the amplitude of the pressure peaks were all different from each other, where the largest amplitude was obtained using the highest pressure wave celerity (1000 m/s).

To ensure that the CFD results (Flow-3D model) are mesh independent a mesh convergence study was performed. This study was performed for the pressure traces at midway of pipe 3 using three mesh sizes, which results are shown in Fig. 6. The mesh sizes used in the study were 797,400, 2,694,465 and 6,000,000 cells, respectively. As can be observed in Fig. 6, mesh convergence is approximately achieved using the intermediate mesh size (2,694,465 cells). The CFD results presented in this section and the next one (similar to the present test case) were obtained using a mesh of 6,000,000 cells.

The initial water surface levels for this test are presented in Fig. 5(b). As can be observed in Figs. 5(a) and 5(b), the initial zero-velocity water pools in each pipe are separated by two sluice gates located at the downstream end of each inflowing pipe. The boundary conditions at the upstream end of the inflowing pipes (pipes 1 and 2) and at the downstream end of the outflowing pipe (pipe 3) were assumed to be zero-flux boundaries, which represent a dead-end pipe. The transient flow is obtained after an instantaneous and simultaneous opening of the sluice gates at time $t = 0$. It is pointed out that this hypothetical test case and the next (three-way dividing flow) assume a perfect venting condition (e.g., no air entrapment is allowed).

The opening of the sluice gates generated a free surface flow surge at the upstream end of pipe 3 that moved in the downstream direction. The continuous supply from the inflowing pipes into the outflowing pipe (pipe 3) pressurized the upstream end

of pipe 3 converting the free surface flow surge into an open channel-pressurized flow positive interface that moved in the downstream direction. Once this positive interface reached the downstream end (dead-end) the whole pipe 3 was pressurized and remained that way during the entire simulation. At the inflowing pipes (pipes 1 and 2), the flow remained fully free surface during the entire simulation, although some wave reflections originated at their boundaries (dead-end and junction pond) were observed during the visualization of the simulations. The simulated piezometric depth traces mid-way of pipes 2 (results for pipe 1 are the same as pipe 2 because of symmetry) and 3 are presented in Figs. 7 and 8, respectively. The simulation time for this test case was 12 seconds, however for pipe 3 (Fig. 8) which involves pressurized flows (high frequency of oscillations) the results are shown only for the first 2.8 seconds for better visualization. The simulated results using the proposed approach were obtained using 200 cells in each pipe and a maximum Courant number of Cr = 0.8.

The results for pipe 2 (Fig. 7), the flow regime of which remained in free surface conditions during the entire simulation, show a good agreement between the proposed approach and CFD model for the frequency and amplitude of the piezometric depth trace at mid-way of this pipe. The accurate modeling of free surface flows is not a problem for most models intended for transient flows in mixed flow conditions (one or two sets of equations). Hence, the focus of the comparison in this section is under mixed and pressurized flow conditions.

As mentioned earlier, pipe 3 undergoes a flow type change from free surface flow to mixed flow to pressurized flow. For this pipe, the frequency of the pressure oscillation (pressurized flow) obtained with the proposed model is 1.01 times that of the CFD model (with acoustic wave model). The amplitude of the first pressure oscillation peak (pressurized flow) obtained with the proposed model is 0.8 times that of

the CFD model (with acoustic wave model). The amplitude of the second pressure oscillation peak (pressurized flow) obtained with the proposed model is 1.07 times that of the CFD model (with acoustic wave model). These results and Fig. 8 show a good agreement between the proposed approach and the CFD with acoustic wave model in pressurized flow conditions. However, this location (mid-way of pipe 3) is pressurized slightly earlier when using the proposed model. Discrepancies in the results (proposed and CFD) are expected since a one-dimensional model has much more limitations than a three-dimensional model. The phase difference between the proposed and CFD model results for the pressure oscillations may not be important as long as the frequency and amplitude of the pressure oscillations are similar.

Fig. 8 also shows the CFD results without using the acoustic wave model. As can be observed, the results for the piezometric depth obtained using this approach are much smaller than those of the proposed model and the CFD with acoustic wave model. Thus, the compressibility of the flow (associated with the propagation of acoustic waves) is very important when simulating pressurized transient flows. For simulating free surface flows, considering compressibility of the flow is not important as they produce identical results.

Three-way dividing flow

The hypothetical test presented in this section considers a three-way dividing flow system which is depicted in Fig. 9(a). As shown in Fig. 9(a), all pipes have a length of 5 m, the junction pond has a diameter of 1 m, the inflowing pipe (pipe 1) has a diameter of 0.6 m and the outflowing pipes (pipes 2 and 3) have both a diameter of 0.5 m. The Manning's roughness coefficient used in the 1D simulation is 0.015 $m^{1/6}$, the head loss coefficient assumed at the inlet and outlet of the pond is 0.5,

the waterhammer wave speed considered is 100 m/s and the initial flow velocity in all pipes is 0 m/s. A waterhammer wave speed of 100 m/s rather than 1000 m/s was used for the same reasons as explained in the previous test case. The number of cells used in the CFD simulation was about 6,000,000 and the output time was 0.001 seconds.

The initial water levels for this test are presented in Fig. 9(b). As can be seen in Figs. 9(a) and 9(b), initially the upstream water pool (pipe 1) is separated from the downstream water pools (pipes 2 and 3) by a sluice gate located immediately upstream of the junction pond. The boundary conditions at the upstream end of pipe 1 and at the downstream end of pipes 2 and 3 were assumed to be zero-flux boundaries. The transient flow was produced after an instantaneous opening of the sluice gate at time $t = 0$.

The opening of the sluice gate generated two free surface flow surges at the upstream end of pipes 2 and 3 that moved downstream in the respective pipes. Shortly thereafter, the water supply from the inflowing pipe (pipe 1) into the outflowing pipes (pipes 2 and 3) pressurized and depressurized intermittently the upstream end of pipes 2 and 3 creating positive and negative open channel-pressurized flow interfaces at the upstream end of these pipes. Shortly after, the upstream end of pipes 2 and 3 were fully pressurized, which created positive open channel-pressurized flow interfaces that moved downstream in the respective pipes. Once these positive interfaces reached the downstream end (dead-end) the entire pipes 2 and 3 were pressurized and remained that way during the entire simulation. At the inflowing pipe, the flow remained fully free surface during the entire simulation, although some wave reflections originating at its boundaries (dead-end and junction pond) were observed during the visualization of the simulations. The simulated piezometric depth traces mid-way of pipes 1 and 2 are presented in Figs. 10 and 11,

respectively. The simulation time for this test case was 16 seconds, however for pipes 2 and 3 (Fig. 11) that involve pressurized flows the results are shown only for the first 3.6 seconds. The simulated results using the proposed approach were obtained using 200 cells in each pipe and a maximum Courant number of Cr = 0.8.

In a similar way to the previous test case, the results for pipe 1 (Fig. 10), which flow regime remained in free surface conditions during the entire simulation, show a good agreement between the proposed approach and CFD model for the frequency and amplitude of the piezometric depth trace at mid-way of this pipe.

As mentioned earlier, pipe 2 undergoes a flow type change from free surface flow to mixed flow to pressurized flow. For this pipe, the frequency of the pressure oscillation (pressurized flow) obtained with the proposed model is 1.03 times that of the CFD model (with acoustic wave model). The amplitude of the second pressure oscillation peak (pressurized flow) obtained with the proposed model is 1.01 times that of the CFD model (with acoustic wave model). These results and Fig. 11 show a good agreement between the proposed approach and the CFD model (with acoustic wave model) in pressurized flow conditions. As can be observed in Fig. 11, pressure oscillations between t = 2 and 2.5 seconds are simulated using the CFD with acoustic wave model. These oscillations are the result of local pressurization due to fluctuation of free surface flow waves near the crown of pipe 2. At about t = 2.5 seconds, the location under analysis (mid-way of pipe 2) was fully pressurized. The results in Fig. 11 also show that the dissipation rate of the pressure oscillations simulated using the CFD model (with acoustic wave model) is slightly faster than that of the proposed model. Fig. 11 also shows the CFD results without using the acoustic wave model. As in the previous test case, the results for the piezometric depth obtained using this approach are much smaller than those of the proposed model and the CFD with acoustic wave model.

Oscillation tube

This test case examines a drop-shaft connected to a single-horizontal pipe for simulating pressurized flows in a drop-shaft subjected to a rapid variation of its water surface level. With the aim of evaluating the drop-shaft boundary in pressurized conditions physical as well as CFD modeling results were used. The experimental setup, the layout of which is depicted in Fig. 12 (a), was built in the Ven Te Chow Hydrosystems Laboratory of the University of Illinois at Urbana-Champaign. It consisted of a 4.98 m long horizontal plexiglass pipe connected at its upstream and downstream ends by a 2.2 m long vertical pipe of the same material as the horizontal pipe. The inside diameter of all pipes was 50.8 mm (2”). At the center of the horizontal pipe, a quarter-turn ball valve was installed, which as shown in Fig. 12 (b), separated the initial water levels upstream and downstream of the valve. The length of the vertical pipes was intentionally chosen to be of the same scale as the horizontal pipe so that the vertical flow has a clear effect on the results. The water levels in the upstream vertical pipe (left vertical pipe in Fig. 12) were recorded using a Canon GL2 color video camera. For a better visualization of the water levels, the water in the oscillation tube was previously dyed. The acquired images were post-processed using the Image Processing Toolbox of MATLAB. For the MATLAB analysis, the video images were converted first to gray-scale images that in turn were converted to black and white images (binary system: 1 = black and 0 = white). The water level for each image was determined by computing the maximum row that has a pixel with a value of 1.

To ensure that the results of the OpenFOAM CFD code were mesh independent a mesh convergence study was performed and the results are shown in Fig. 13. The mesh sizes used in the study were 32,352, 71,100 and 112,229 cells, respectively.

Mesh convergence was achieved using the intermediate mesh size (71,100 cells). The CFD results presented in this section were obtained using a mesh of 112,229 cells.

The transient flow in the experiments was obtained by a rapid opening of the valve, which created periodic oscillations of water surface levels in the vertical pipes. The measured and simulated water level traces at the upstream vertical pipe (left vertical pipe in Fig. 14) are presented in Fig. 14. The simulated results using the proposed and "mass/energy" approach were obtained using 400 cells, a pressure wave celerity of 1000 m/s, a Manning roughness coefficient of 0.010 $m^{1/6}$ (typical for a plexiglass pipe), a Courant number of Cr = 0.8 and neglecting the head losses across the valve. The results in Fig. 14 labelled "mass/energy" are obtained with the ITM model using the steady energy equation instead of the momentum equation.

The water level oscillation frequency obtained with the proposed, "mass/energy" and CFD models are 1.02, 1.22 and 1.01 times that of the experiment, respectively. The amplitude of the first oscillation peak obtained with the proposed, "mass/energy" and CFD models are 0.99, 0.99 and 1.03 times that of the experiment, respectively. These results show a good agreement for the frequency and amplitude of water level oscillations between the proposed approach, CFD model, and measured results. However, the oscillation frequency obtained with the "mass/energy" approach is significantly different (22%) from that of the experiment. Hence, it appears that when the lengths of near-horizontal pipelines or tunnels are of the same order of magnitude of the lengths of drop-shafts (vertical pipes), the inertia of the flow in the drop-shafts needs to be taken into account for the accurate prediction of the frequency of water surface levels in drop-shafts. However, in most large sewer systems, the lengths of near-horizontal pipelines or tunnels are much larger than the lengths of drop-shafts. In the latter case, ignoring the vertical momentum or includ-

ing it will yield similar results.

Conclusions

This paper presents a junction and drop-shaft boundary conditions (BCs) for one-dimensional modeling of transient flows in single-phase conditions (pure liquid). The BCs are formulated for the case when mixed flows are simulated using two sets of governing equations, the Saint Venant equations for the free surface regions and the compressible water hammer equations for the pressurized regions. The proposed BCs handle all possible flow regimes and their combinations. The flow in each pipe can range from free surface to pressurized flow and the water depth at the junction or drop-shaft can take on all possible levels. The BCs are applied to the following three cases: a three-way merging flow, a three-way dividing flow and a drop-shaft connected to a single-horizontal pipe subjected to a rapid variation of the water surface level in the drop-shaft. The accuracy of these test cases are evaluated using two Computational Fluid Dynamics (CFD) models. For the third case, laboratory results as well as CFD results were used for evaluating its accuracy. The key results are as follows:

(1) The formulated boundary conditions were used with good success for accurately simulating all possible flow regimes in all tested cases.
(2) The equations of Guo and Song (1991) for simulating pure pressurized flows in drop-shafts (vertical shafts) were reformulated to overcome numerical instabilities produced when using this approach.
(3) When the lengths of near-horizontal pipelines or tunnels are of the same order of magnitude of the lengths of drop-shafts (vertical pipes), the inertia of the flow in the drop-shafts needs to be taken into account for the accurate pre-

diction of the frequency of water surface levels in drop-shafts. However, in most large sewer systems, the lengths of near-horizontal pipelines or tunnels are much larger than the lengths of drop-shafts. In the latter case, ignoring the vertical momentum or including it will yield similar results.

(4) Overall, the presented junction and drop-shaft boundary conditions can be used for modeling transient free surface, pressurized, and mixed flow conditions with good accuracy.

Acknowledgments

This work was conducted at the University of Illinois at Urbana-Champaign as part of the studies for the Tunnel and Reservoir Plan (TARP) Modeling Project in Chicago, Illinois. The authors gratefully acknowledge the Metropolitan Water Reclamation District of Greater Chicago for their financial support. The third author wish to acknowledge the Hong Kong Research Grant Council, Project No. 613407. Special thanks to MSc. Andrew Waratuke and Dr. Octavio Sequeiros for their assistance on the experimental work and to Engineer Nils Oberg for his assistance on the video image processing analysis. Last but not least our special thanks to the anonymous manuscript reviewers for their insightful comments and suggestions.

Notation

A = cross-sectional area of flow;

a = pressure wave celerity;

A_f = full cross-sectional area of the conduit;

c = gravity wave celerity;

Cr = Courant number;

D = Drop-shaft diameter;

d = conduit diameter;

dr = drop height between pipe invert and junction bottom;

g = acceleration due to gravity;

H = Piezometric depth at any location;

k = local head loss coefficient;

n_m = Manning roughness coefficient;

Q = Flow discharge;

Q_d = inflow discharge that enters the junction pond at its top;

Q_o = overflow discharge;

s = wave speed;

T = top width;

t = time;

u = flow velocity;

y_b = Piezometric depth at a pipe boundary;

y_c = critical depth;

y_d = piezometric depth at section 1;

y_u = flow depth right upstream the junction boundary;

y_{conj} = conjugate depth associated with y_u;

ρ = fluid density at atmospheric pressure;

ρ_f = fluid density in pressurized flow conditions;

Subscripts

b = boundary.

Superscripts

n = old time step;

$n + 1$ = new time step.

References

Bourdarias, C., Gerbi, S., 2007. A finite volume scheme for a model coupling free surface and pressurised flows in pipes. Journal of Computational and Applied Mathematics 209 (1), 109–131.

Capart, H., Bogaerts, C., Kevers-Leclercq, J., Zech, Y., 1999. Robust numerical treatment of flow transitions at drainage pipe boundaries. Wat. Sci. Tech. 39 (9), 113–120.

Capart, H., Sillen, X., Zech, Y., 1997. Numerical and experimental water transients in sewer pipes. J. Hydraul. Research 35 (5), 659–672.

Cardle, J. A., 1984. An investigation of hydraulic transients in combination free surface and pressurized flows. Ph.D. thesis, Univ. of Minnesota, Twin Cities, MN.

Flow Science, I., 2005. Flow-3d v. 9.0 user's manual. Tech. rep., Flow Science Inc., Santa Fe, N.M.

Garcia-Navarro, P., Priestley, A., Alcrudo, F., 1994. An implicit method for water flow modeling in channels and pipes. J. Hydraul. Research 32 (5), 721–742.

Guo, Q., Song, C. S., 1991. Dropshaft hydrodynamics under transient conditions. Journal of Hydraulic Engineering 117 (8), 1042–1055.

Hirt, C. W., 1985. Volume-fraction techniques: Powerful tools for flow modeling. In: Flow Sci. Rep. FSI-92-00-02. Washington, D.C.

Hirt, C. W., Sicilian, J. M., 1985. A porosity technique for the definition of obstacles in rectangular cell meshes. In: Proceedings 4th Int. Conf. Ship Hydro. Washington, D.C.

Jasak, H., 1996. Error analysis and estimation for the finite volume method with application to fluid flows. Ph.D. thesis, Imperial College of Science, Technology and Medicine, United Kingdom.

León, A. S., 2006. Improved modeling of unsteady free surface, pressurized and mixed flows in storm-sewer systems. Ph.D. thesis, Univ. of Illinois at Urbana-Champaign, Urbana, IL.

León, A. S., Ghidaoui, M. S., 2010. "Discussion of numerical oscillations in pipe-filling bore predictions by shock-capturing models" by Jose G. Vasconcelos, Steven J. Wright and Philip L. Roe. Journal of Hydraulic Engineering, In print.

León, A. S., Ghidaoui, M. S., Schmidt, A. R., García, M. H., 2006. Godunov-type solutions for transient flows in sewers. Journal of Hydraulic Engineering 132 (8), 800–813.

León, A. S., Ghidaoui, M. S., Schmidt, A. R., García, M. H., 2008. An efficient second-order accurate shock-capturing scheme for modeling one- and two-phase water hammer flows. Journal of Hydraulic Engineering 134 (7), 970–983.

León, A. S., Ghidaoui, M. S., Schmidt, A. R., García, M. H., 2009a. Application of Godunov-type schemes to transient mixed flows. Journal of Hydraulic Research 47 (2), 147–156.

León, A. S., Ghidaoui, M. S., Schmidt, A. R., García, M. H., 2010. A robust two-equation model for transient mixed flows. Journal of Hydraulic Research, In print.

León, A. S., Oberg, N., Schmidt, A. R., García, M. H., 2009b. User's manual of Illinois Transient Model - two equation model. A model for the analysis of transient and non-transient free surface, pressurized and mixed flows in storm-sewer systems. Tech. rep., University of Illinois at Urbana-Champaign.

McInnis, D. A., 1992. Comprehensive hydraulic analysis of complex pipe systems. Ph.D. thesis, Univ. of Toronto, Toronto, Canada.

OpenCFD, 2007. Openfoam user guide. Tech. rep., OpenCFD Ltd., Berkshire, United Kingdom.

Politano, M., Odgaard, A. J., Klecan, W., 2007. Case study: Numerical evaluation

of hydraulic transients in a combined sewer overflow tunnel system. Journal of Hydraulic Engineering 133 (10), 1103–1110.

Ridgway, K. E., Kumpula, G. J., 2006. Surge modeling in sewers using the Transient Analysis Program (TAP), In Contemporary Modeling of Urban Water Systems, Monograph 15. W. James, K. N. Irvine, E. A. McBean, R. E. Pitt, and S. J. Wright, Editors. CHI Publications.

Rodi, W., 1980. Turbulence models and their application in hydraulics. International Association for Hydraulic Research, Delft, The Netherlands.

Sjöberg, A., 1976. Calculation of unsteady flows in regulated rivers and storm sewer systems. Tech. Rep. Division of Hydraulics, Chalmers Univ. of Technology, Goteborg, Sweden.

Song, C. C. S., Cardle, J. A., Leung, K. S., 1983. Transient mixed-flow models for storm sewers. Journal of Hydraulic Engineering 109 (11), 1487–1503.

Toro, E. F., 2001. Shock-capturing methods for free-surface shallow flows. Wiley, LTD, Chichester, U.K.

Vasconcelos, J. G., Wright, S. J., Roe, P. L., 2006. Improved simulation of flow regime transition in sewers: Two-component pressure approach. Journal of Hydraulic Engineering 132 (6), 553–562.

Yen, B. C., 1986. Hydraulics of sewers. Advances in Hydroscience, Urban Storm Drainage 14, 1–115.

Yen, B. C., 1991. Hydraulic resistance in open channels, In Channel Flow Resistance: Centennial of Manning's Formula. Water Resources Publications, Littleton Co, USA.

Yen, B. C., 2001. Hydraulics of sewer systems, in Stormwater collection systems design Handbook. McGraw-Hill.

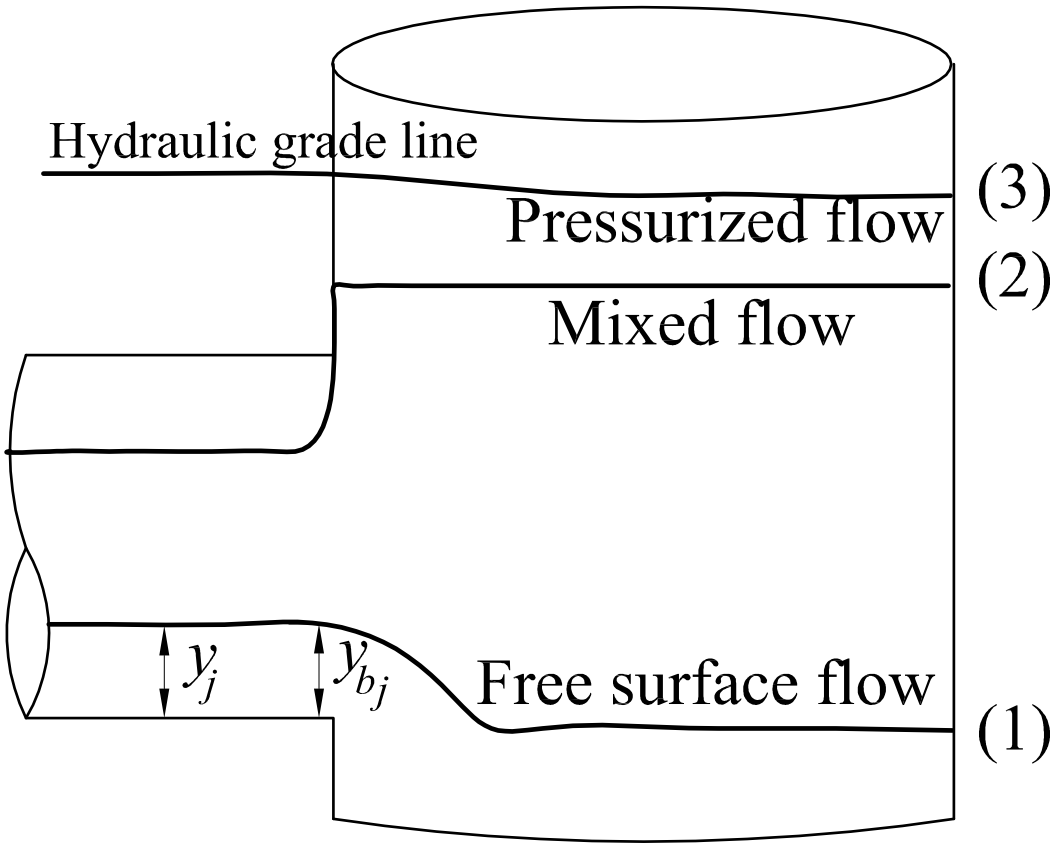

Fig. 1. Sketch of free surface, pressurized and mixed flows

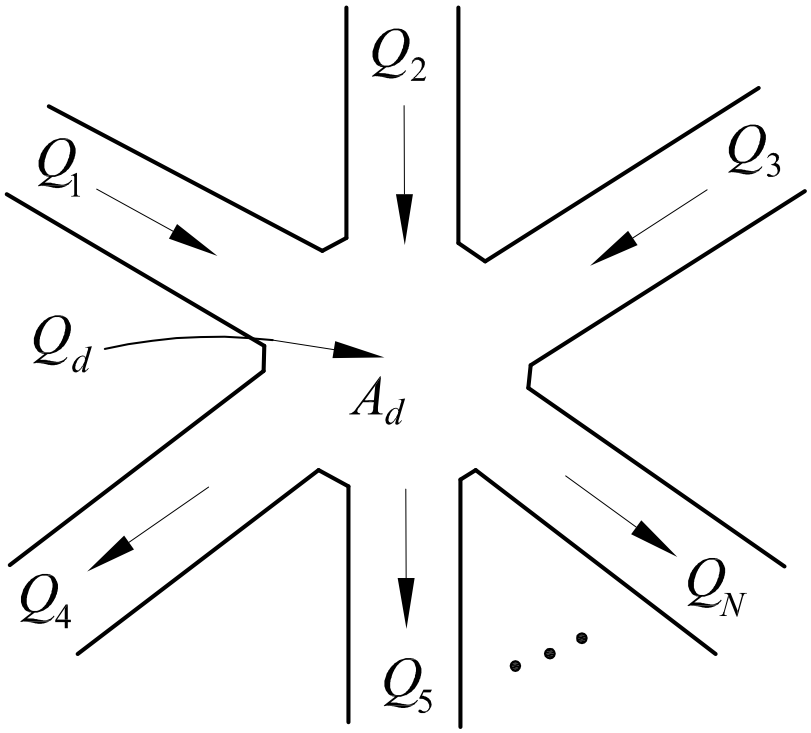

(a)

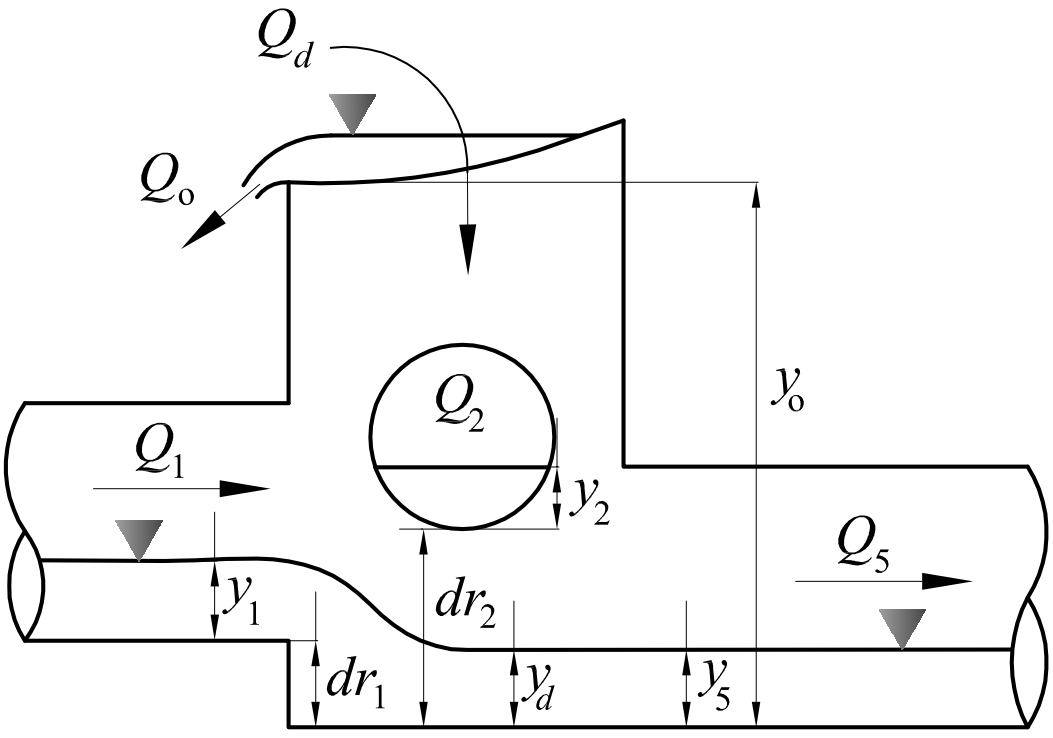

(b)

Fig. 2. Schematic of a N-way junction boundary (a) plan view, (b) side view [To avoid cluttering the side view only pipes 1, 2 and 5 were drawn]

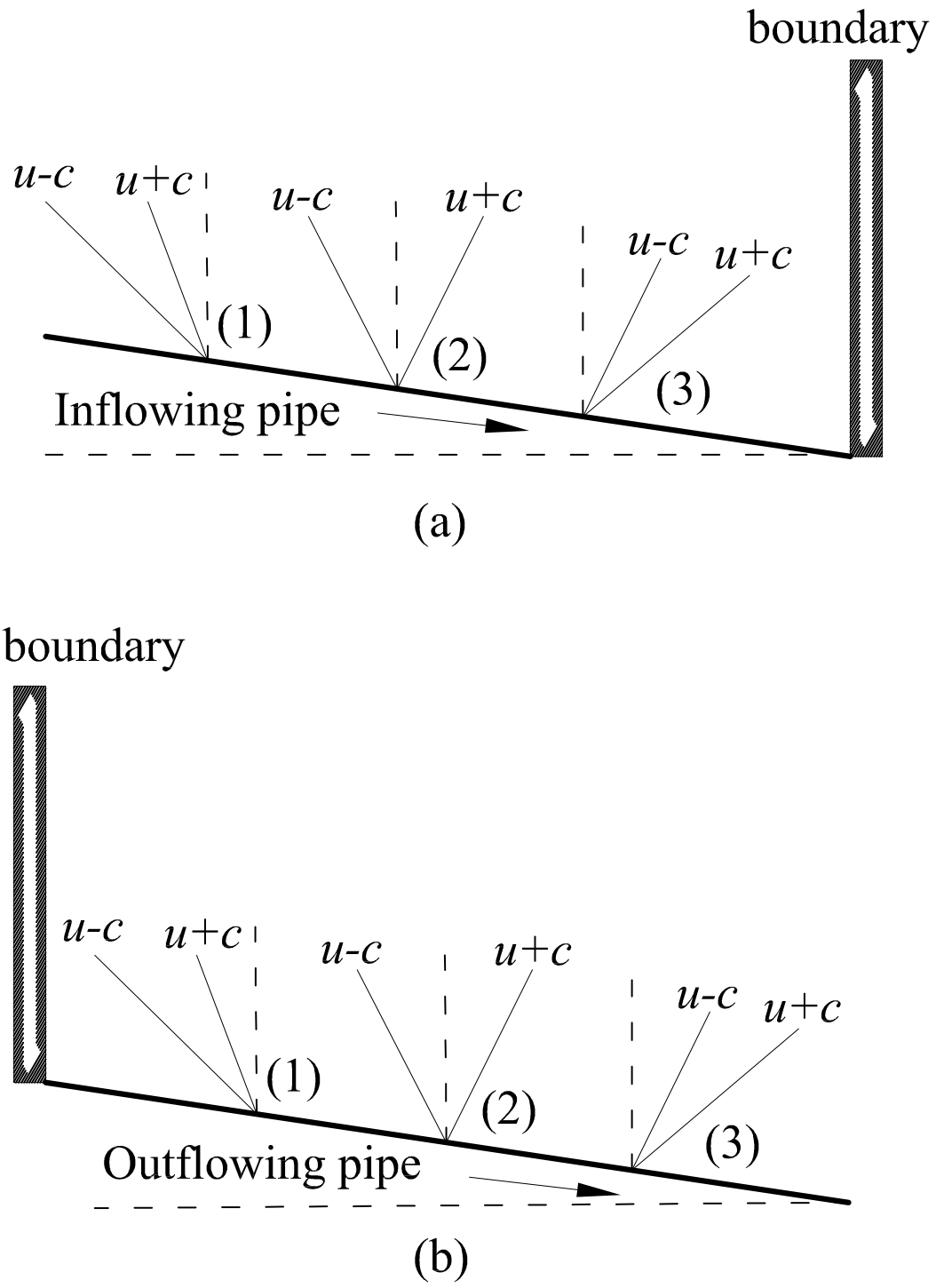

Fig. 3. Characteristic for (a) inflowing and (b) outflowing pipes. Cases: (1) supercritical flow moving upstream, (2) subcritical flow, (3) supercritical flow moving downstream

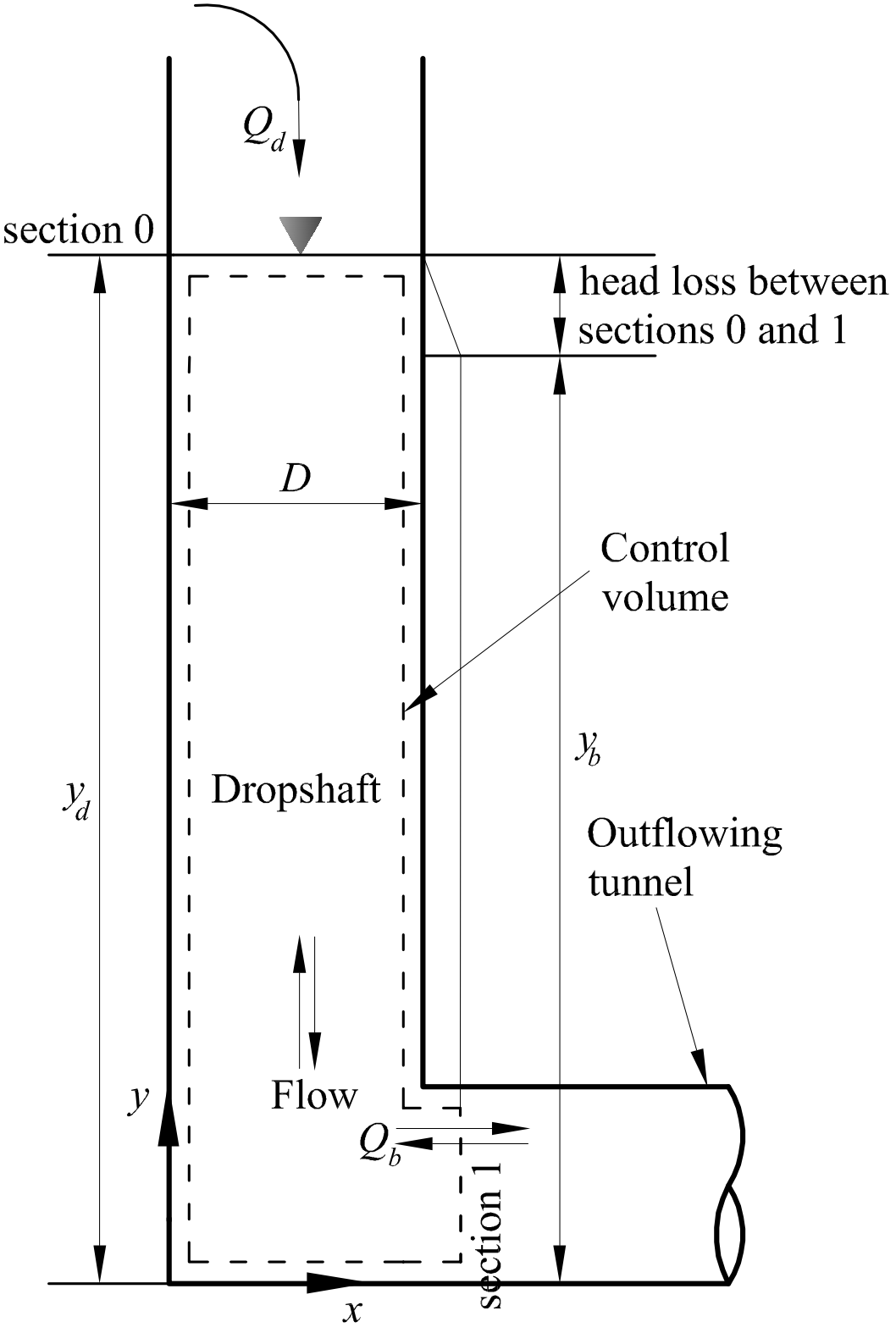

Fig. 4. Schematic of a drop-shaft boundary

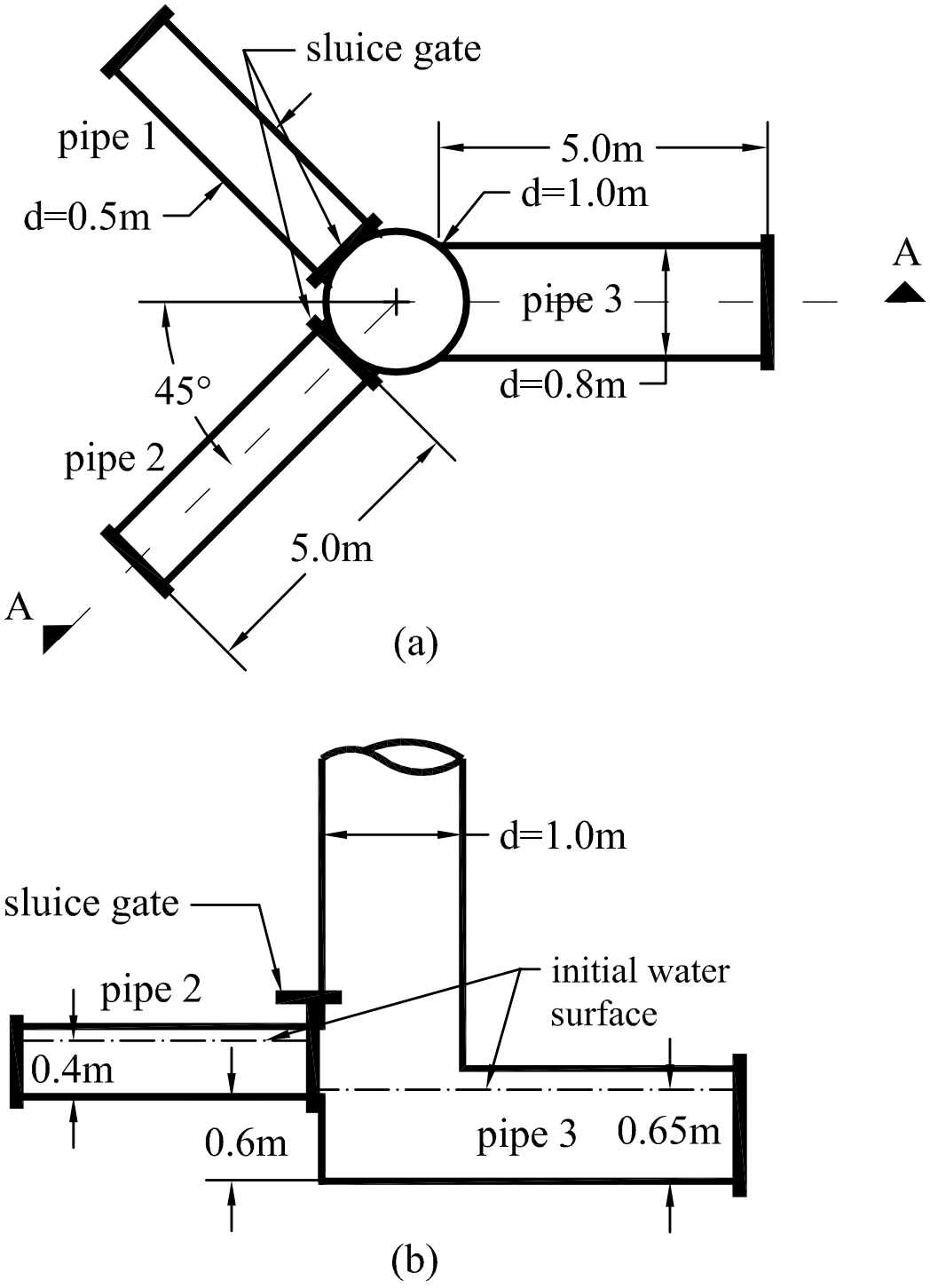

Fig. 5. (a) Plan and (b) section A-A view for three-way merging flow hypothetical case

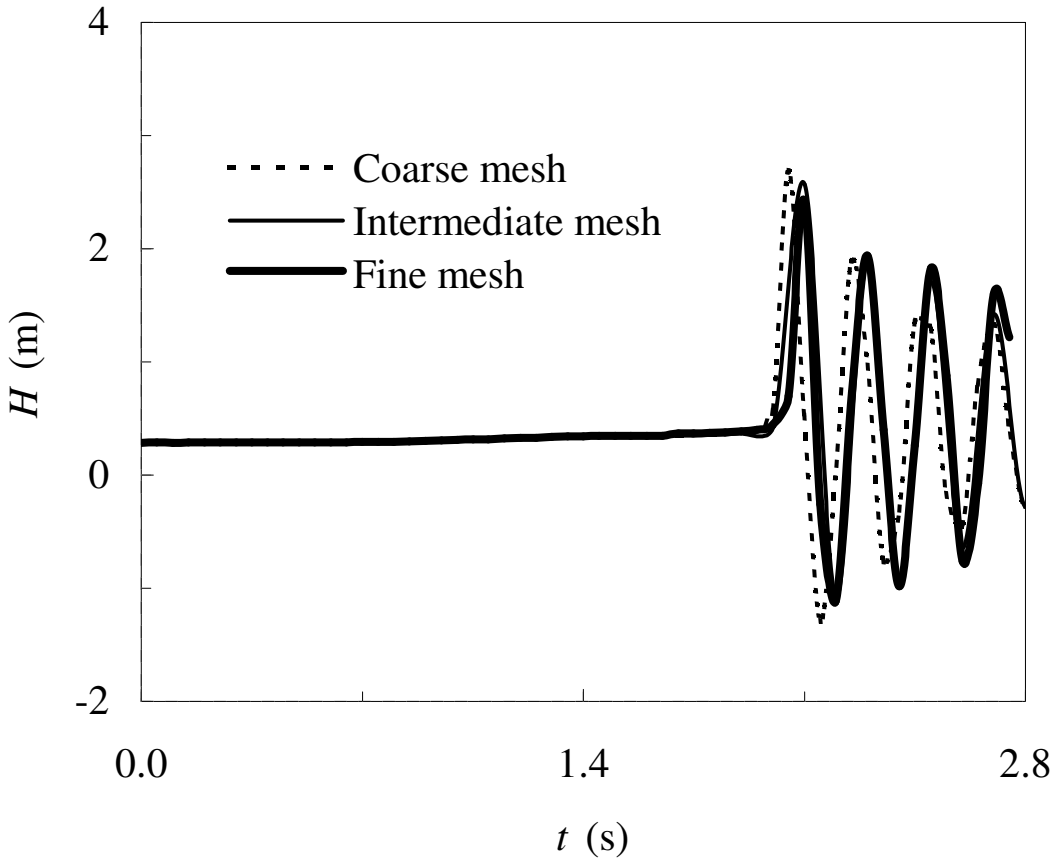

Fig. 6. CFD mesh convergence for three-way merging flow test case (piezometric depth traces at mid-way of pipe 3)

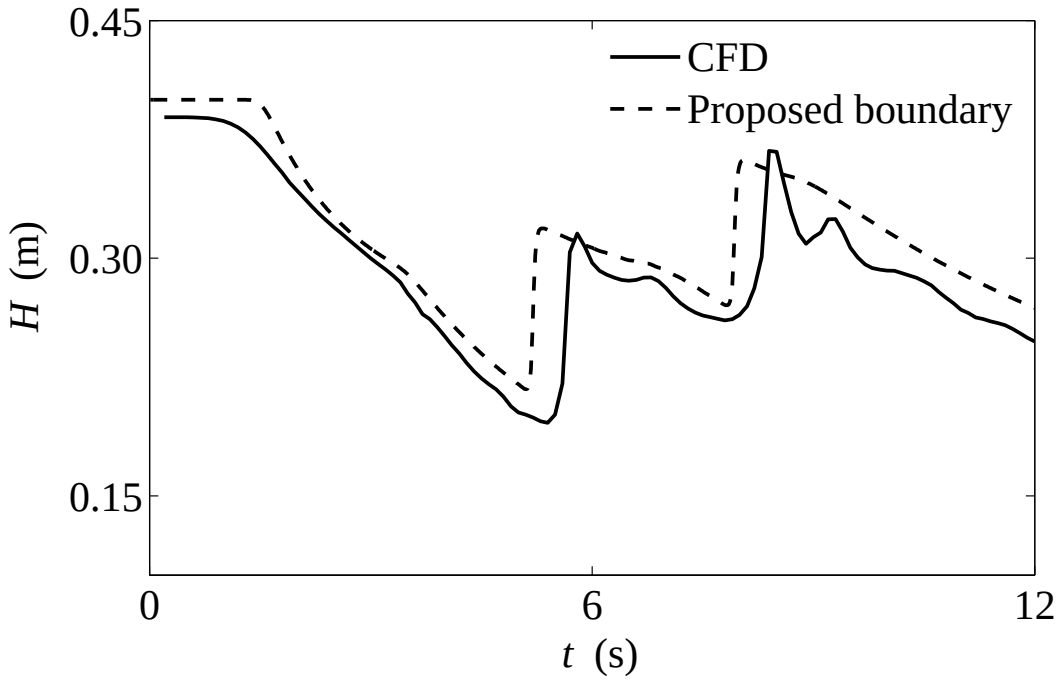

Fig. 7. Piezometric depth trace at mid-way of pipe 2

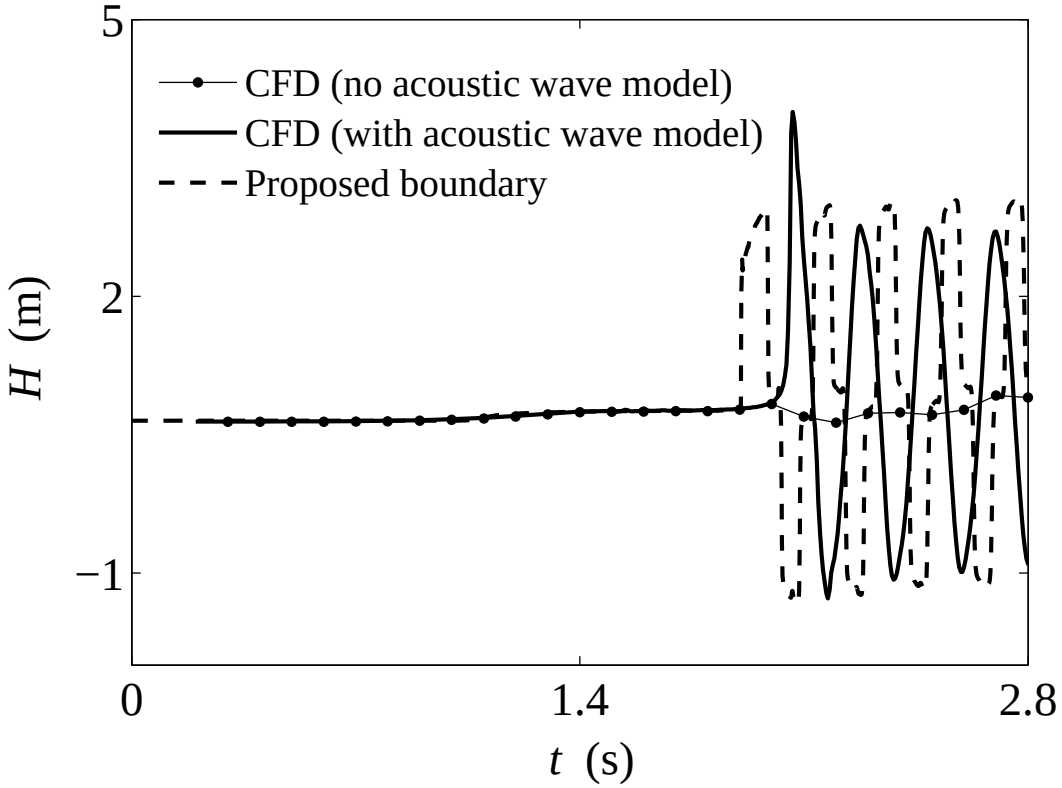

Fig. 8. Piezometric depth trace at mid-way of pipe 3

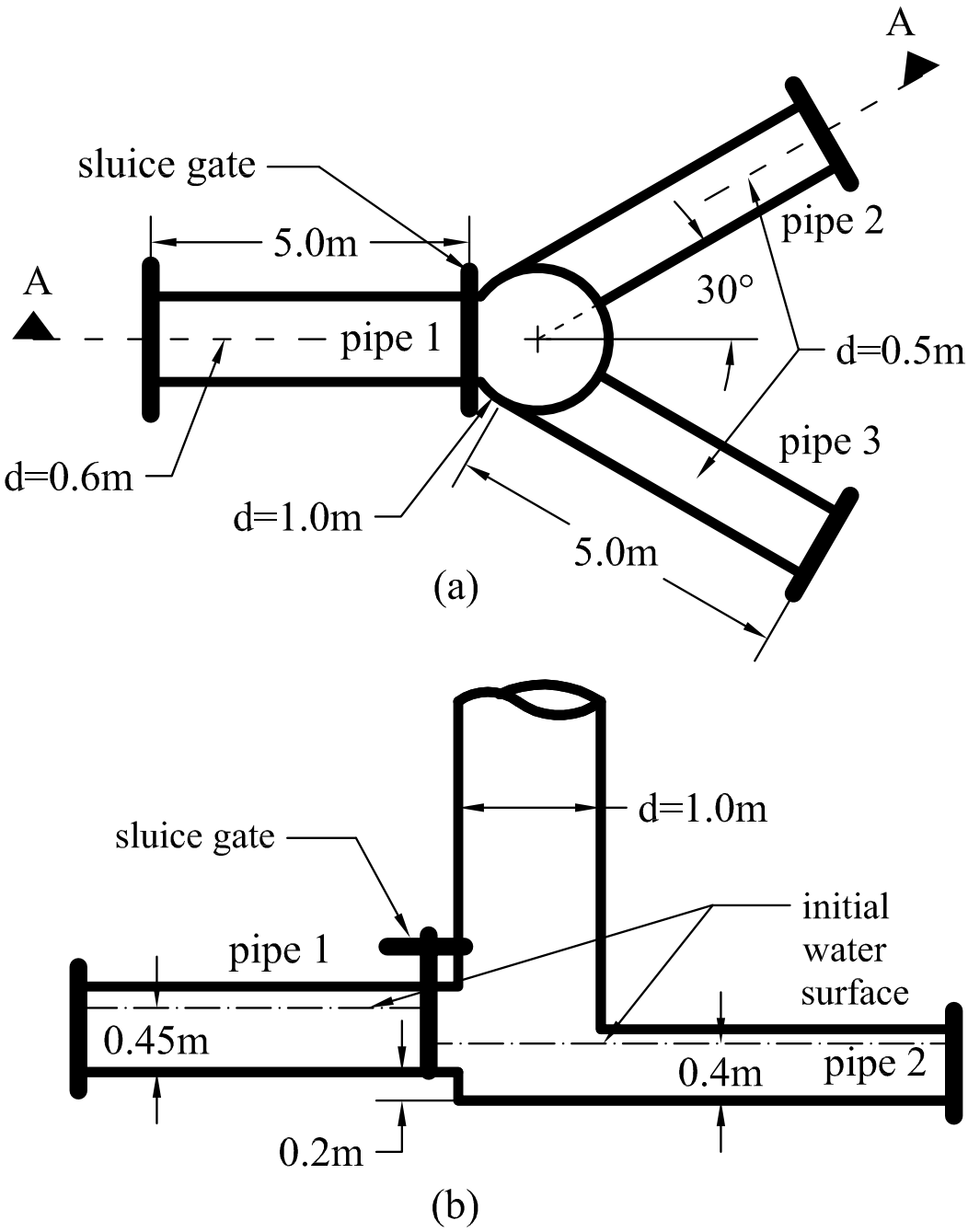

Fig. 9. (a) Plan and (b) section A-A view for three-way dividing flow hypothetical case

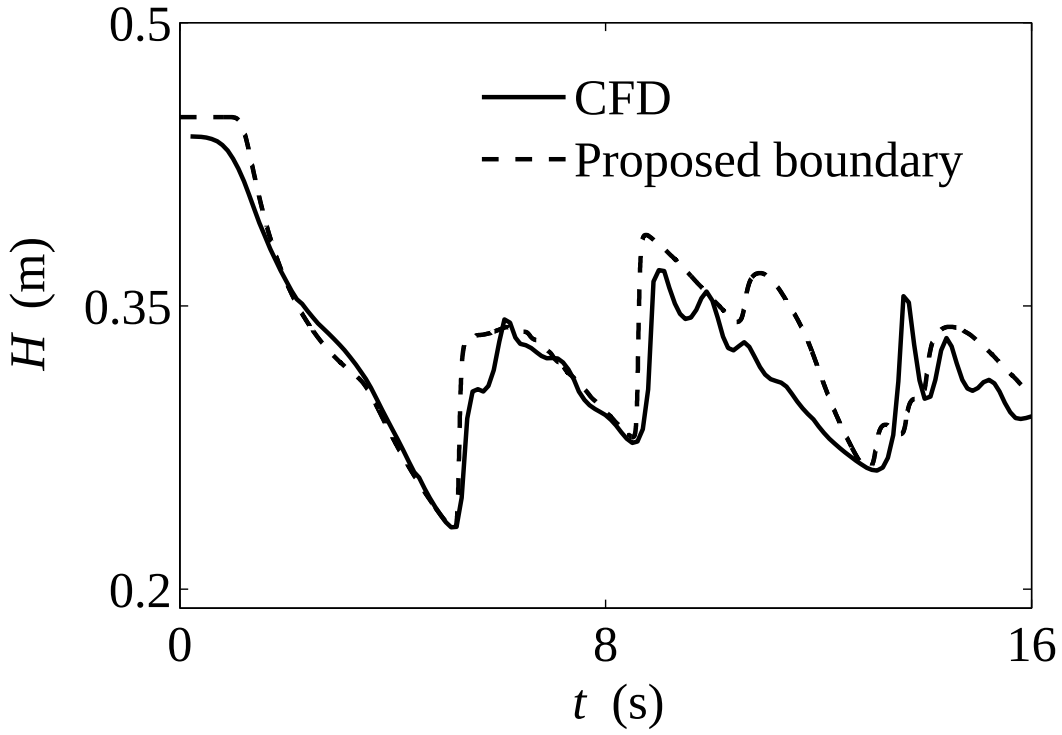

Fig. 10. Piezometric depth trace at mid-way of pipe 1

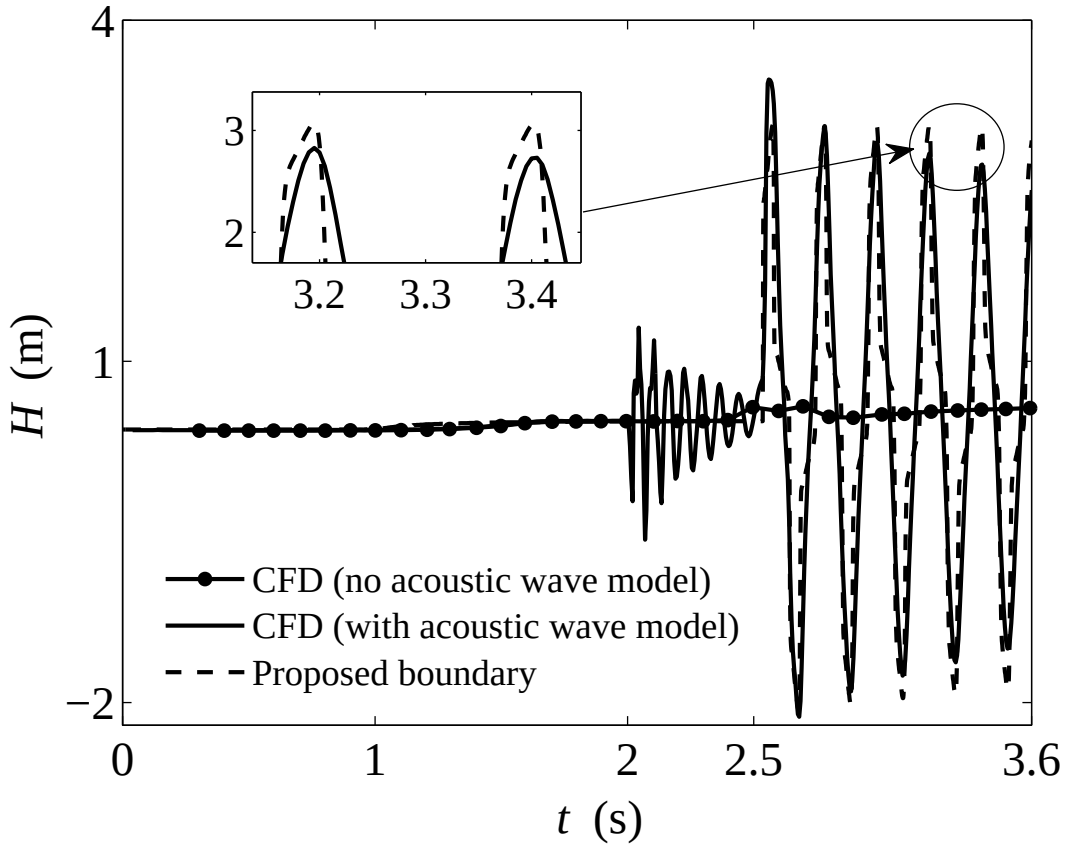

Fig. 11. Piezometric depth trace at mid-way of pipe 2

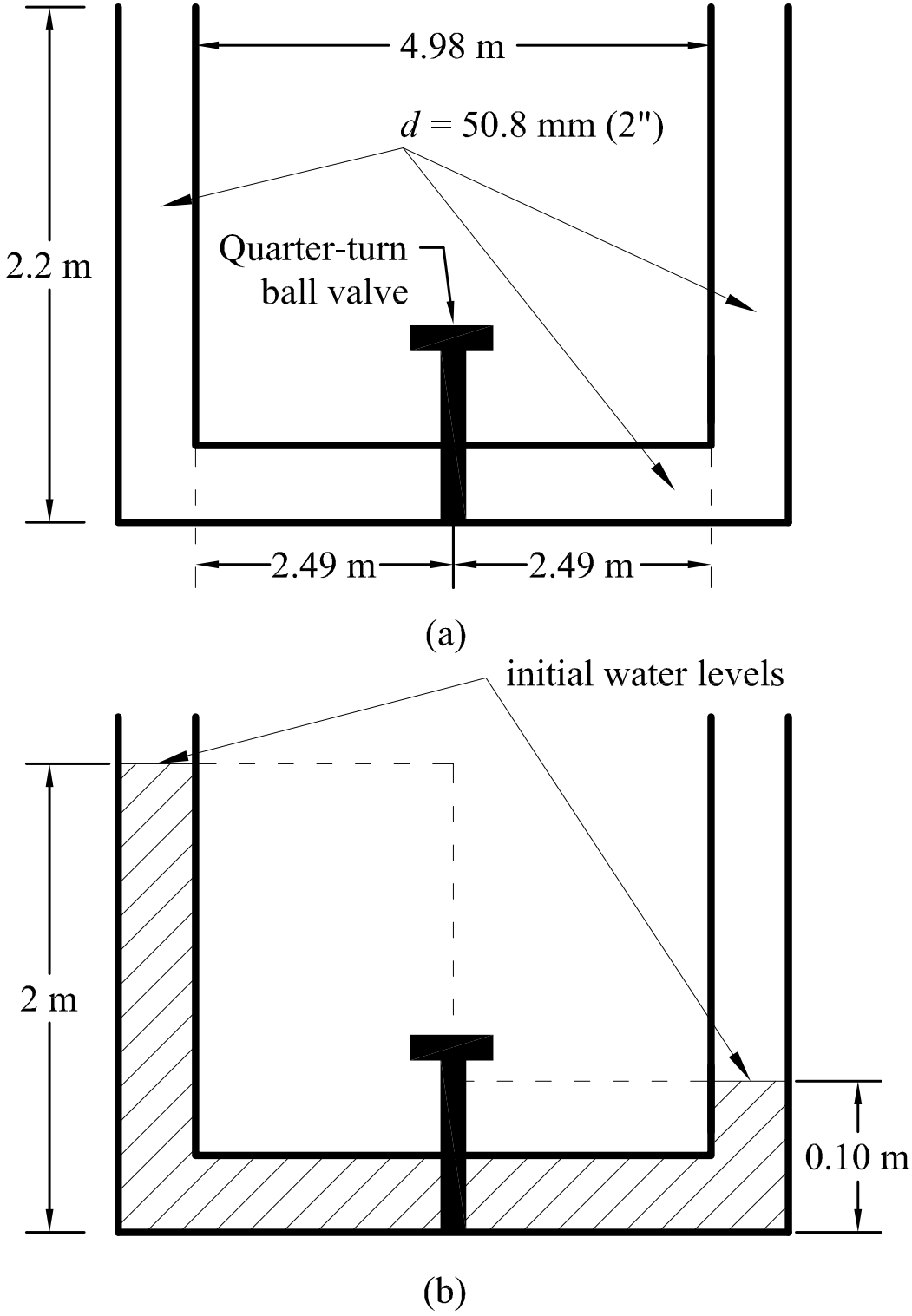

Fig. 12. Experimental setup (not to scale) (a) dimensions and (b) initial water levels

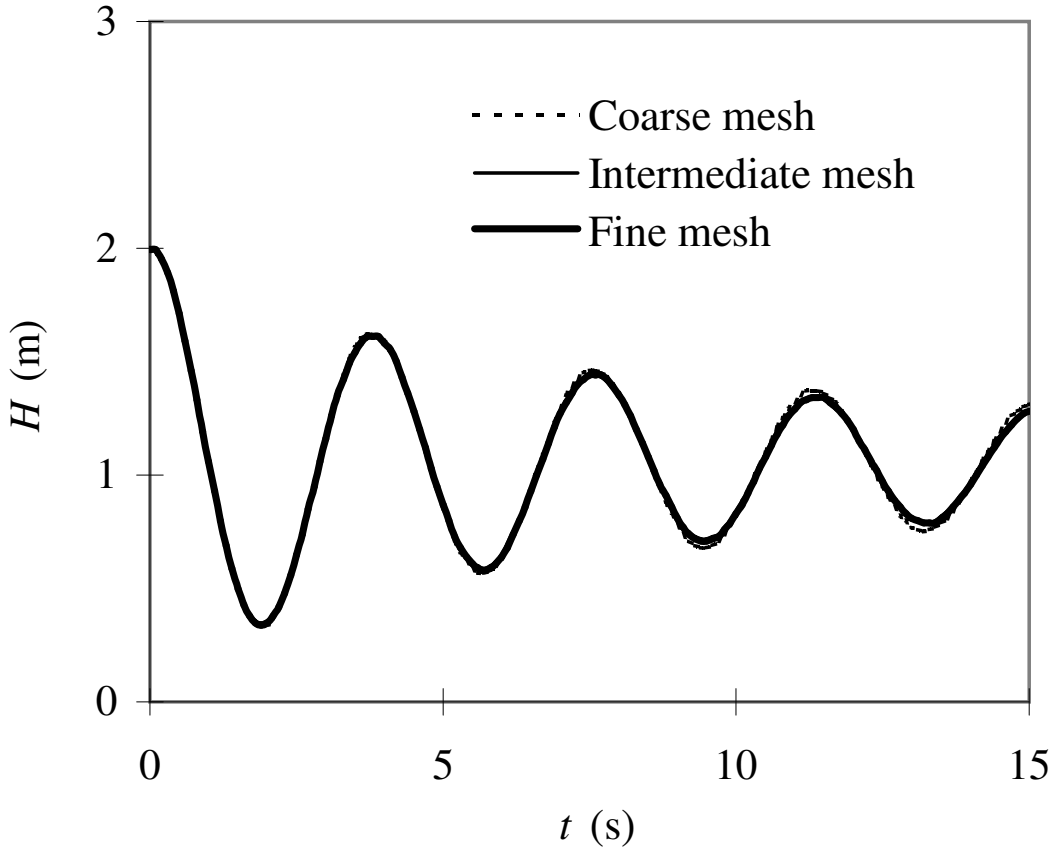

Fig. 13. CFD mesh convergence for oscillation tube test case (Water level elevation at upstream drop-shaft)

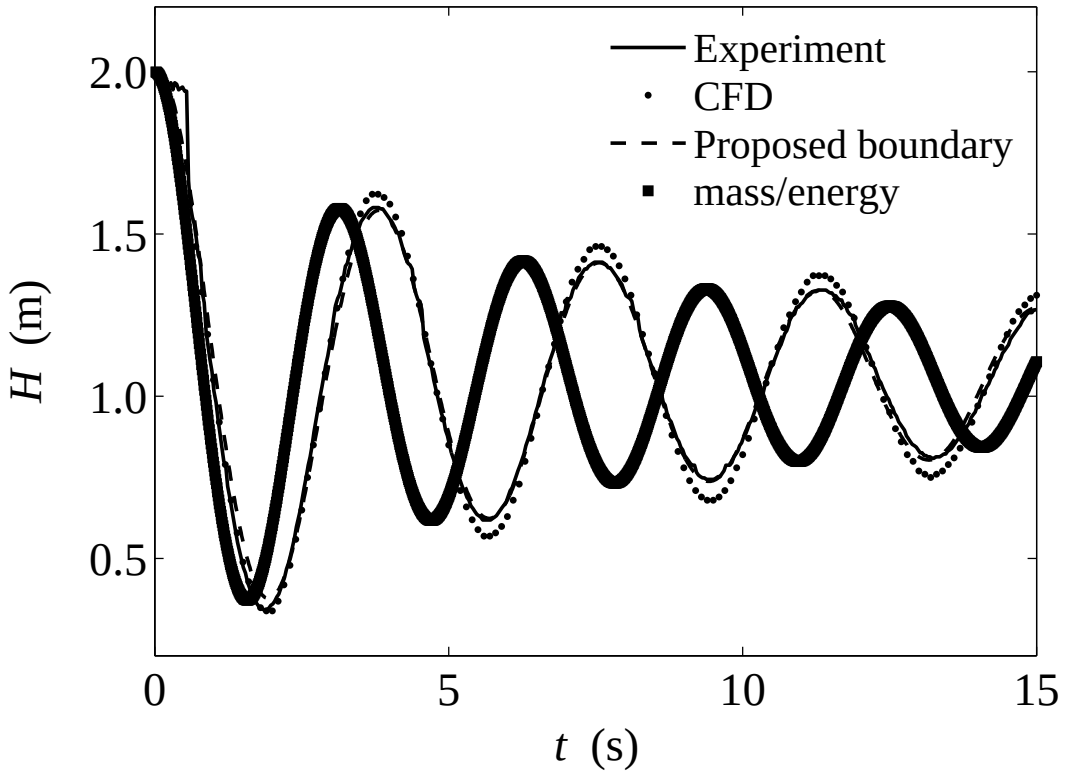

Fig. 14. Water level elevation at upstream drop-shaft